Electronic Supplementary Material (ESI) for Journal of Materials Chemistry A.
This journal is © The Royal Society of Chemistry 2023

Supplementary Information for

Convolutional neural network prediction of the photocurrent−voltage curve directly from scanning electron microscopic image

Yuta Hayashi *et al.*

*Corresponding author. Email:kkata@kc.chuo-u.ac.jp

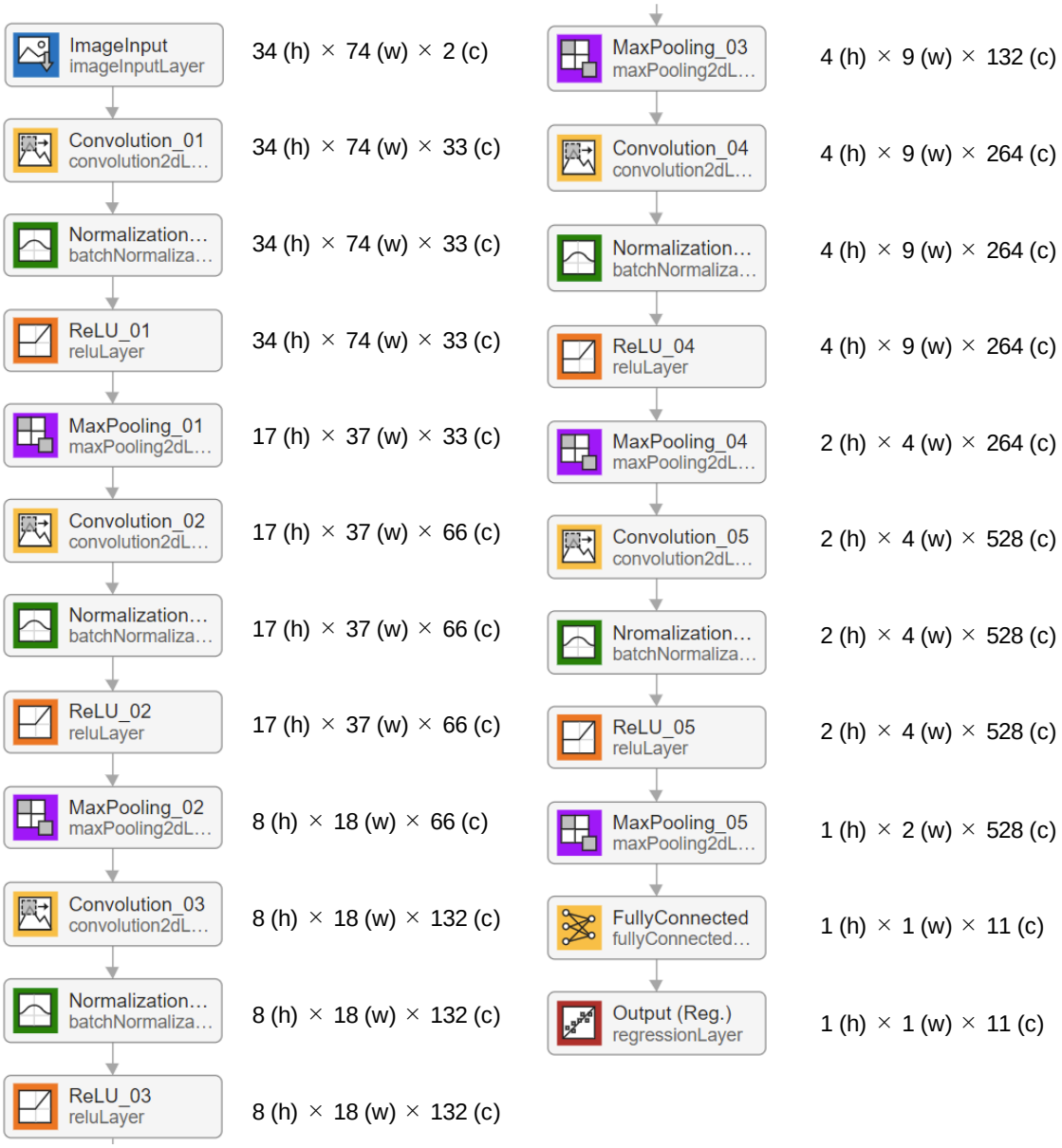

Fig. S1.

The convolutional neural network architecture is provided with an example image input with a size of 34×34×2. Here is an example of the double layers of SEI and BEI images as an input, and the right side provides the data size change at each layer. As a final output, a one-dimensional number array with 11 components is provided. The layers are composed of convolution, normalization, rectified linear unit (ReLU), and pooling layers.

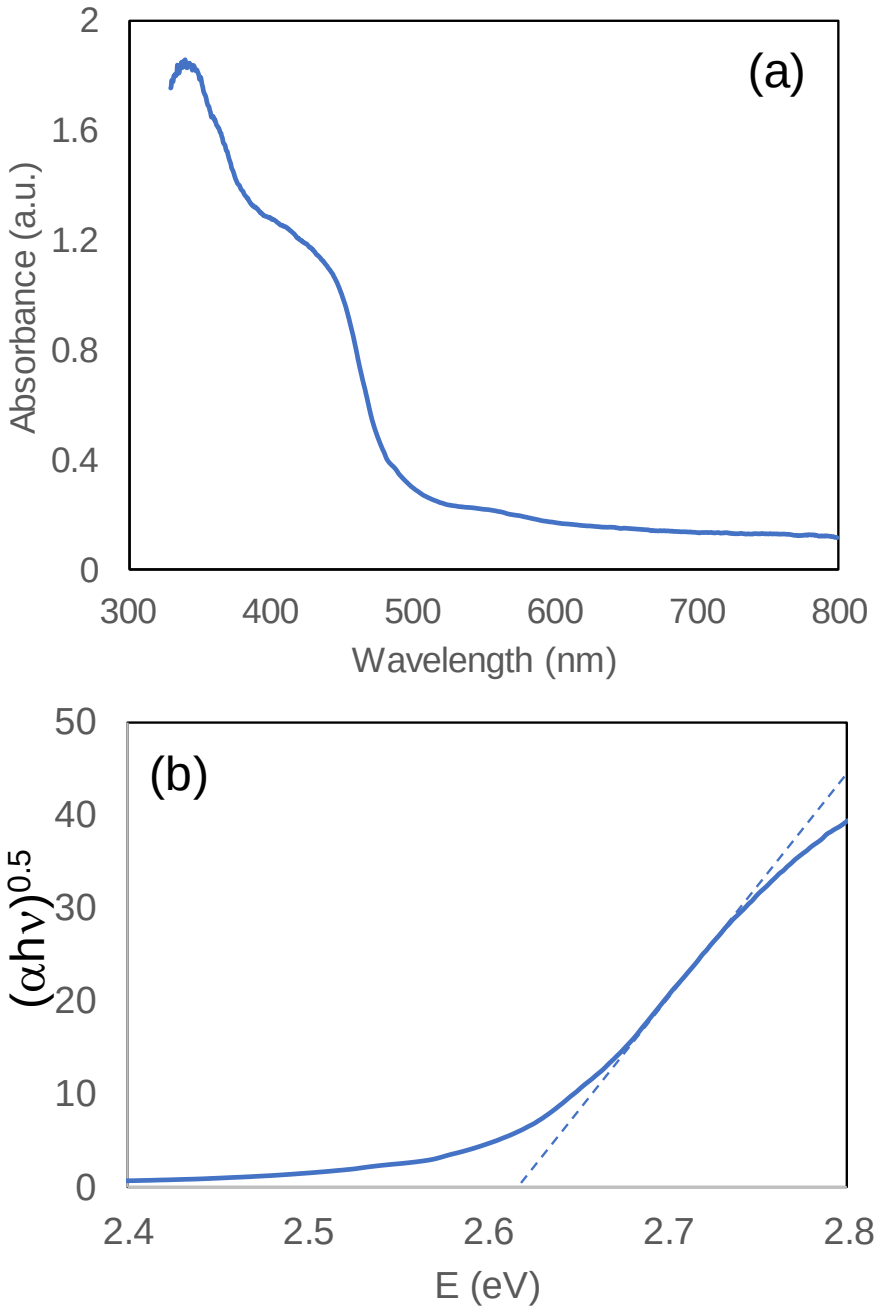

Fig. S2.

UV/Vis absorption spectrum. (a) An example of the absorption spectrum of a $BiVO_4$ photoelectrode is shown. (b) The corresponding Tauc plot is presented. The bandgap of this material corresponded to 2.62 eV.

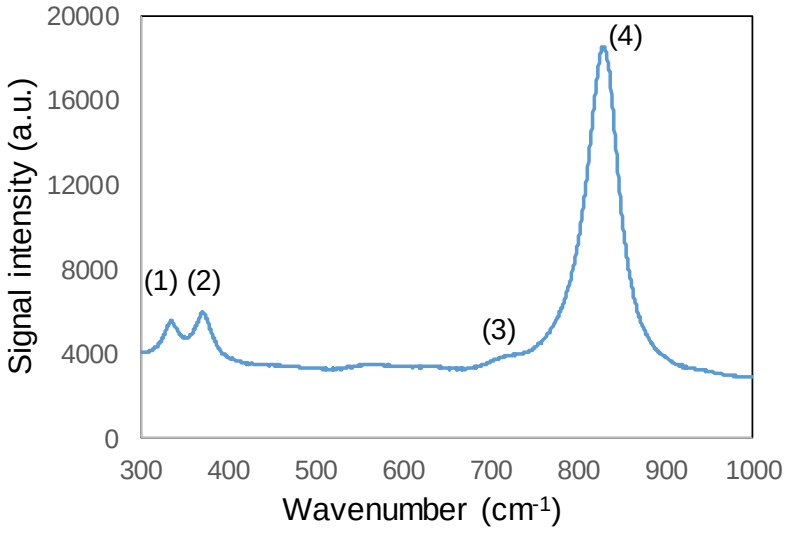

Peak number	Wavenumber (cm-1)	Assignment
1	338	σ_{as} (VO_4^{3-})
2	373	σ_{s} (VO_4^{3-})
3	720	V_{s} (V-O)
4	831	V_{as} (V-O)

(ref) Mali, Sawanta S., Gwang Ryeol Park, Hyungjin Kim, Hyun Hoon Kim, Jyoti V. Patil, and Chang Kook Hong. “Synthesis of Nanoporous Mo:$BiVO_4$ Thin Film Photoanodes Using the Ultrasonic Spray Technique for Visible-Light Water Splitting.” *Nanoscale Advances,* **2019**, 1, 799–806.

Fig. S3.

A Raman spectrum of a $BiVO_4$ photoanode. An example of the Raman spectrum of a $BiVO_4$ film is shown**.** The assignment is summarized in the table.

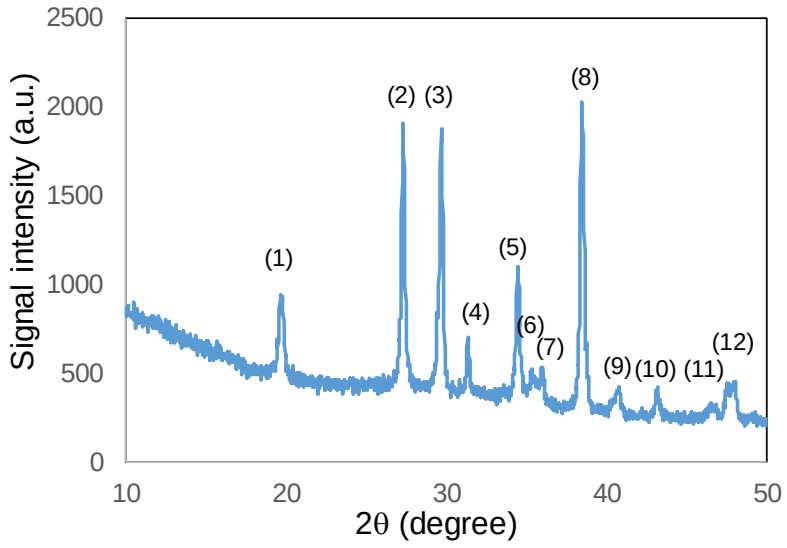

Peak number	Angle	Assignment
1	19.7	(011) and (110) $BiVO_4$
2	27.3	FTO
3	29.7	(121) $BiVO_4$
4	31.3	(040) $BiVO_4$
5	34.5	FTO
6	36.0	(002) $BiVO_4$
7	38.5	FTO
8	40.9	(211) $BiVO_4$
9	43.2	(051) $BiVO_4$
10	46.7	(132) $BiVO_4$
11	47.4	(240) $BiVO_4$
12	48.0	(042) $BiVO_4$

(ref) Pookmanee, Pusit, Suchanya Kojinok, Ratchadaporn Puntharod, Supaporn Sangsrichan, and Sukon Phanichphant. “Preparation and Characterization of BiVO4 Powder by the Sol-Gel Method.” *Ferroelectrics*, 2013, 456, 45–54.

Fig. S4.

An XRD pattern of a $BiVO_4$ photoanode. An example of the XRD pattern of a $BiVO_4$ film is shown**.** The assignment is summarized in the table.

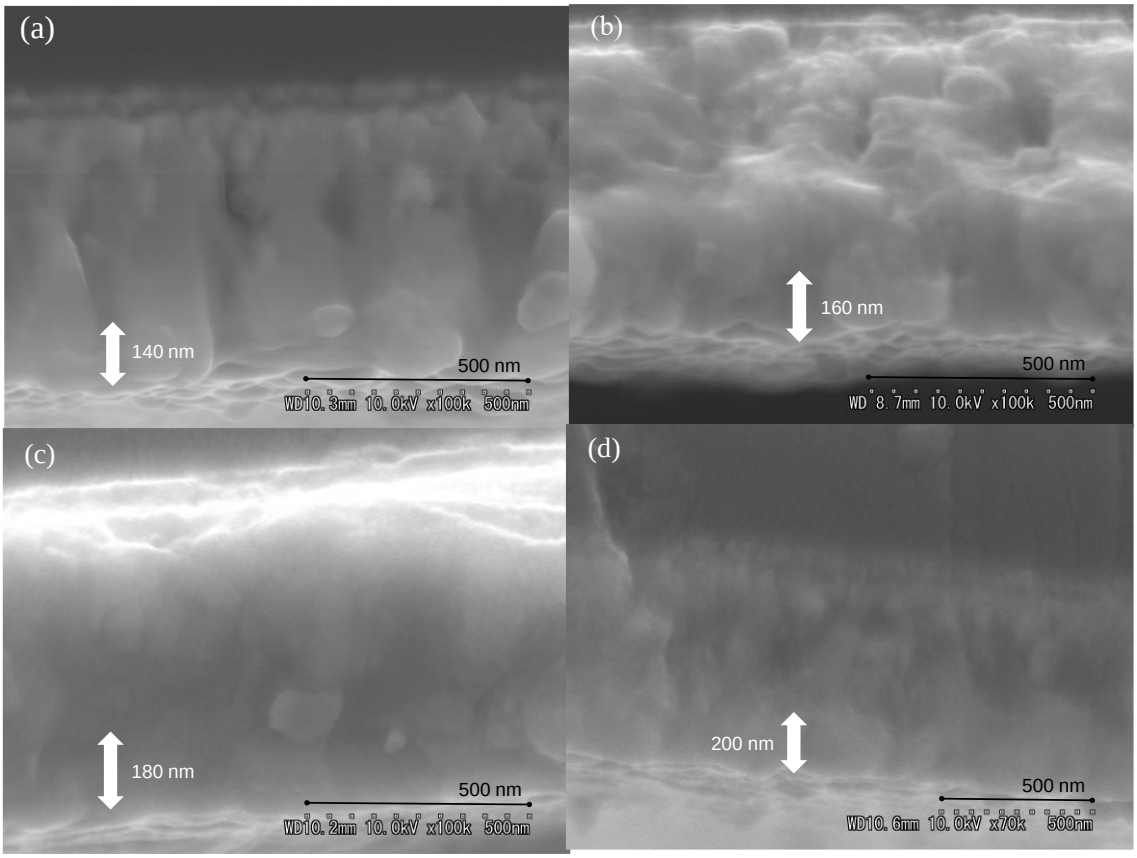

Fig. S5.

The section profiles for the $BiVO_4$ photoelectrodes. The samples were prepared with different spin coating times (a) 9, (b) 11, (c) 13, and (d) 15 times. The white arrows indicate the $BiVO_4$ region.

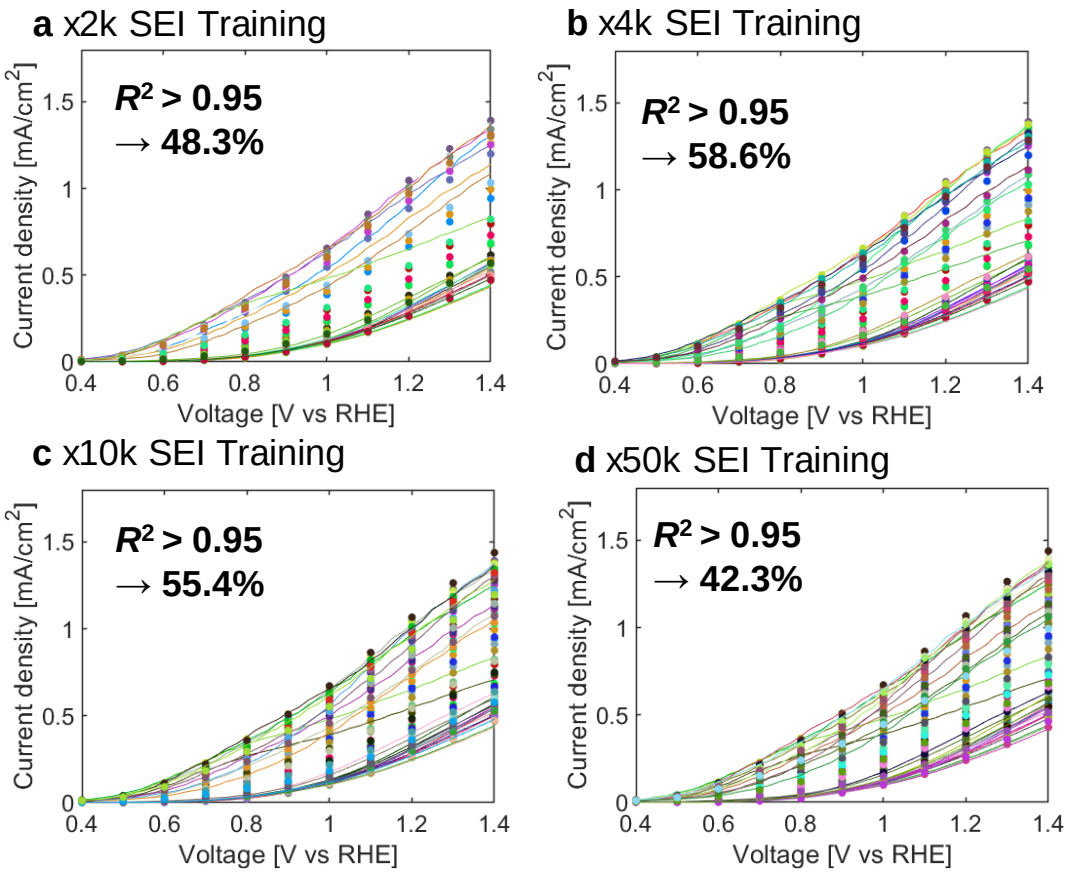

Fig. S6.

The JV curves and the corresponding predicted photocurrent values are shown for the training dataset when different magnifications of SEI images (**a-d**) were used for training the CNN network. 840 images were used for the training and test with a ratio of 8:2. Ten JV curves were randomly selected and were shown with the predicted values. The match ratio (defined by $R^2 > 0.95$) is shown in the figure.

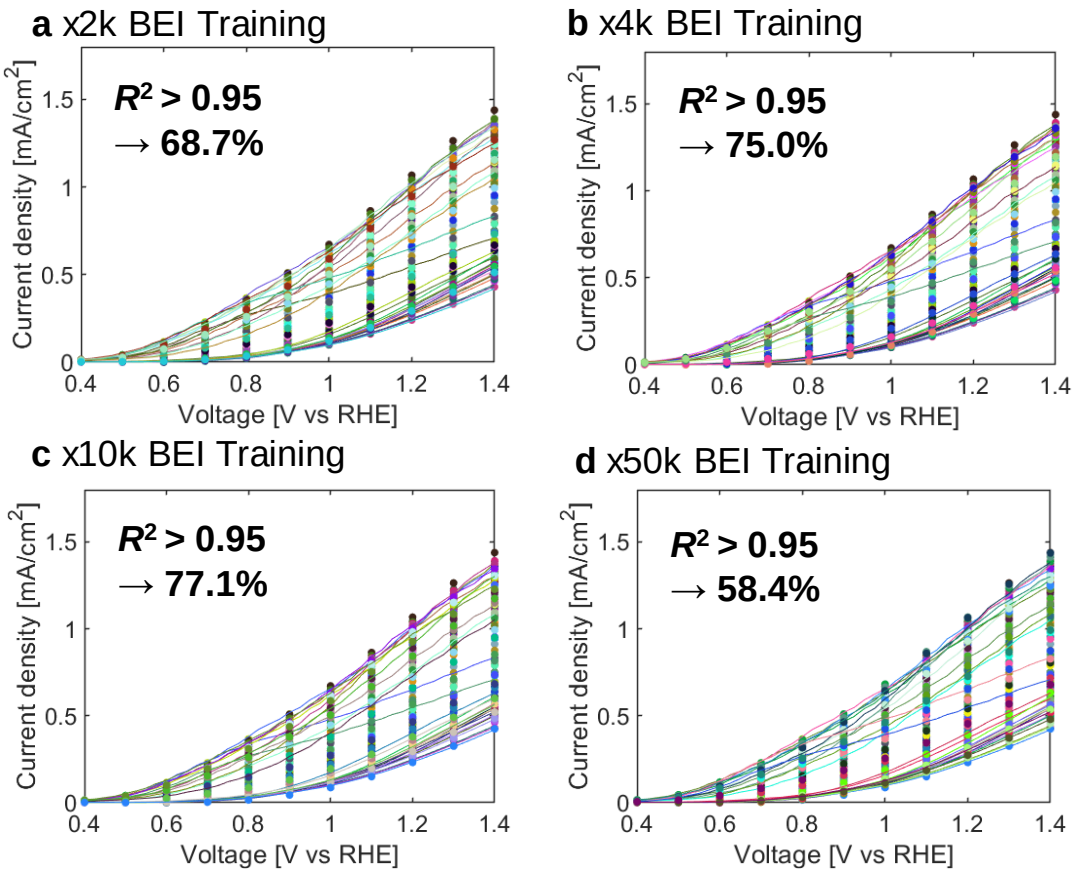

Fig. S7.

The JV curves and the corresponding predicted photocurrent values are shown for the training dataset when different magnifications of BEI images (**a-d**) were used for training the CNN network. 840 images were used for the training and test with a ratio of 8:2. Ten JV curves were randomly selected and were shown with the predicted values. The match ratio (defined by $R^2 > 0.95$) is shown in the figure.

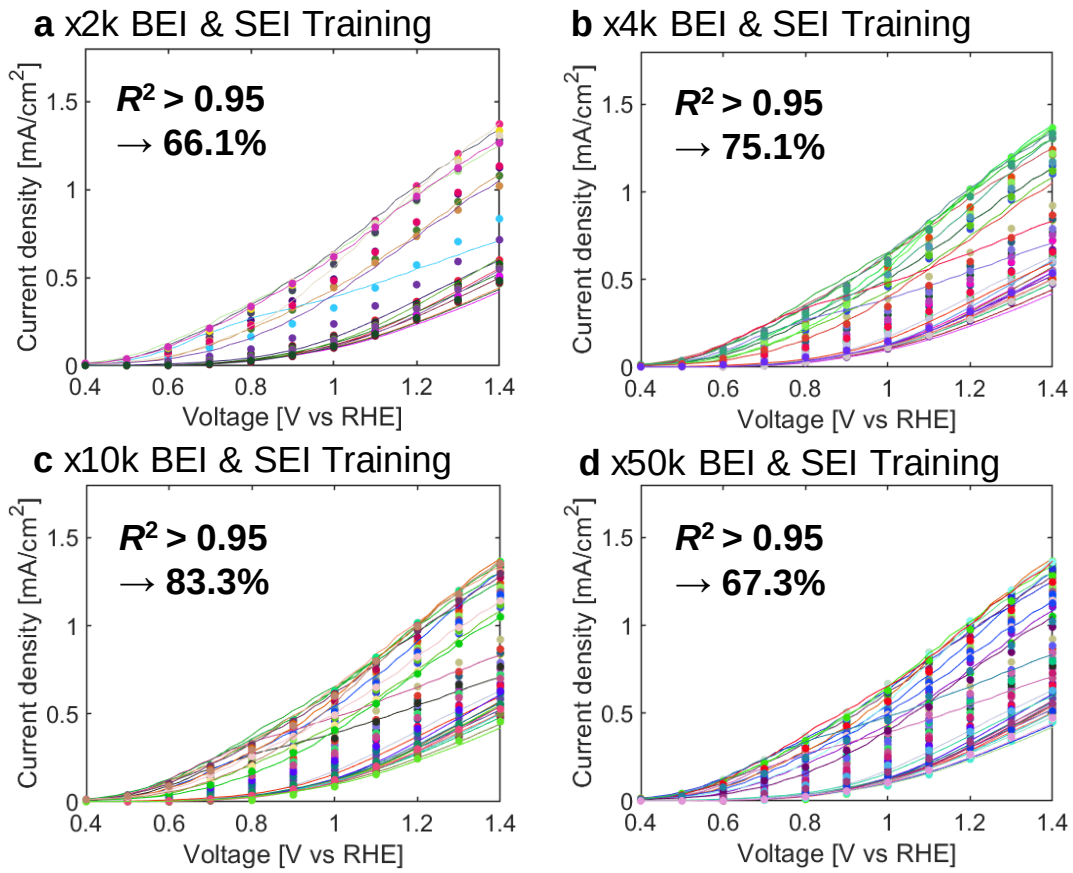

Fig. S8.

The JV curves and the corresponding predicted photocurrent values are shown for the training dataset when different magnifications of SEM images (**a-d**) were used for training of the CNN network. 840 pair of SEI and BEI images were used for the training and test with a ratio of 8:2. The SEM image consisted of an overlaid image with SEI and BEI images. Ten JV curves were randomly selected and were shown with the predicted values. The match ratio (defined by $R^2 > 0.95$) is shown on the figure.

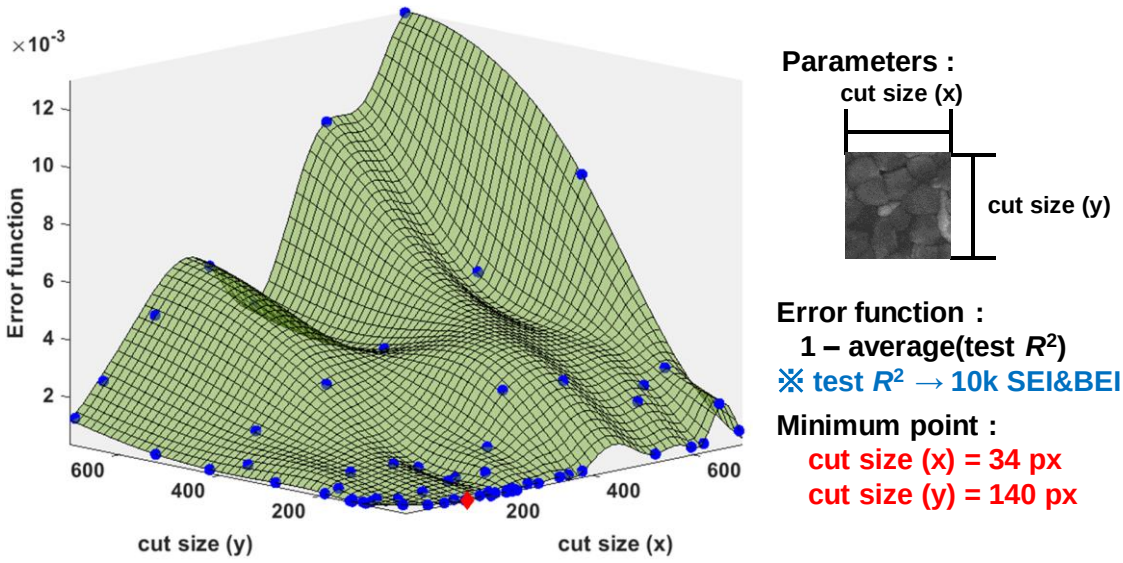

Fig. S9.

The landscape graph is shown during the Bayesian optimization for the hyperparameters; the x and y scales of the cut image size for ×10000 SEM images (overlayer of SEI and BEI images). The cost function was defined as $E(x, y) = 1 - average(R^2)$. The optimized size of the cut image was 34× 140 pixels.

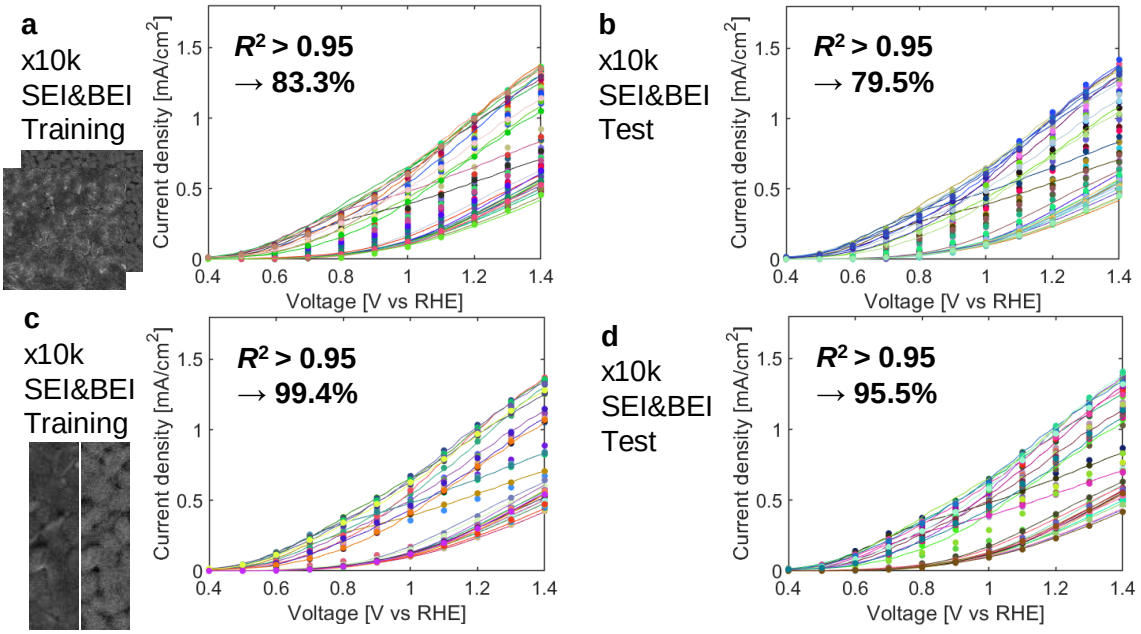

Fig. S10.

The comparison of the prediction ability is shown for the original cut size (256 × 256 pixels) and the optimized cut size by the Bayesian optimization (34 × 140 pixels) for ×10000 SEM images. **a, b** corresponds to the training and test datasets using (256 × 256 pixels), and **c, d** corresponds to the training and test datasets using (34 × 140 pixels). 840 -26,656 images, depending on the cut size, were used for the training and test with a ratio of 8:2. The JV curves and the corresponding predicted photocurrent values are shown for the test dataset. The input data was overlaid images of the SEI and BEI images. Ten JV curves were randomly selected and were shown with the predicted values. The match ratio (defined by $R^2 > 0.95$) is shown in the figure.

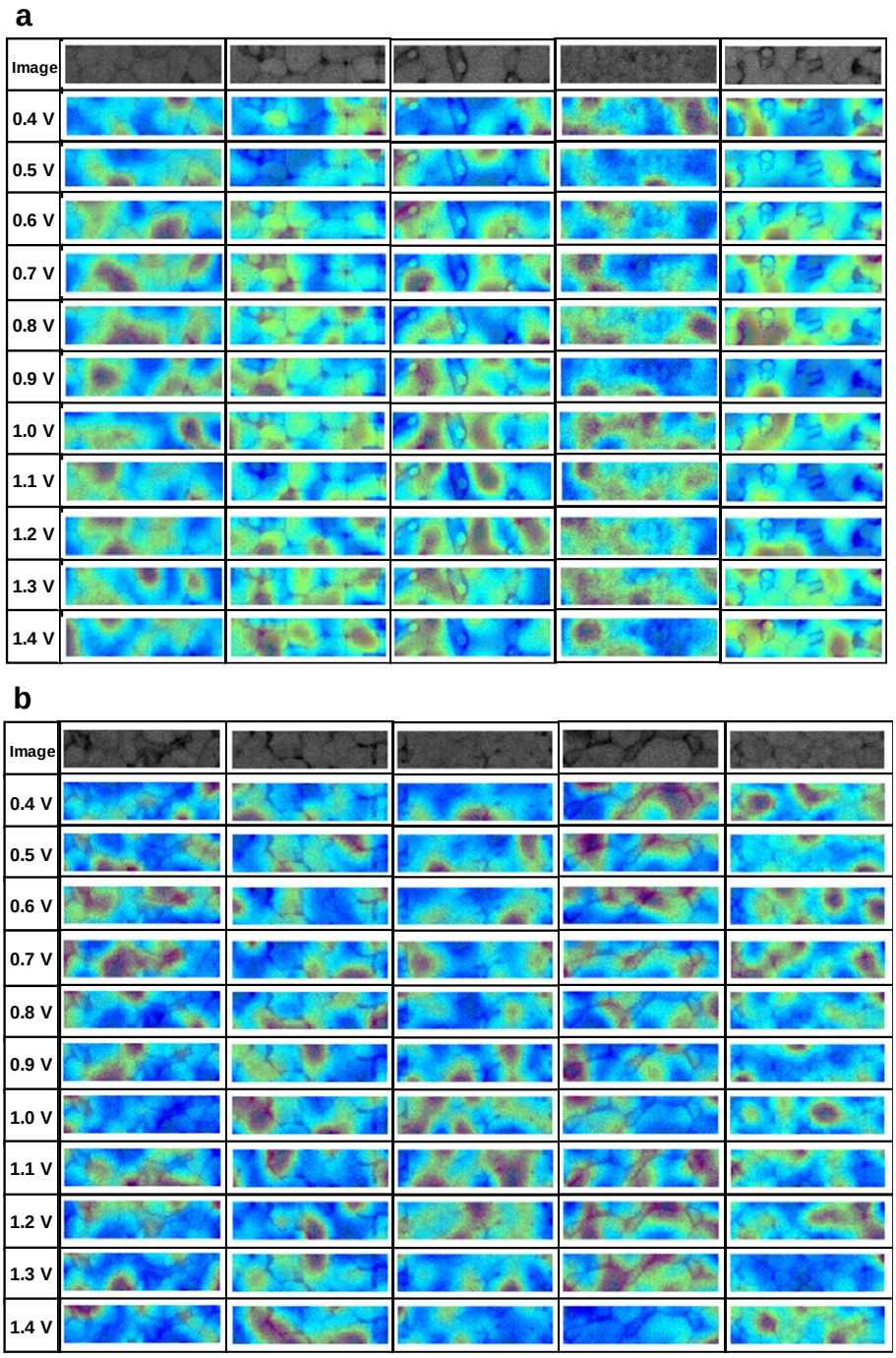

Fig. S11.

LIME activity images are shown for the SEM images (×10000) that provided **a** high and **b** low match ratio (5 sample images for each). The first row shows the original SEM images (BEI) for comparison with the LIME activity images. From top to bottom, the activity images for the prediction of the photocurrent at different bias voltages (0.4 to 1.4 V).

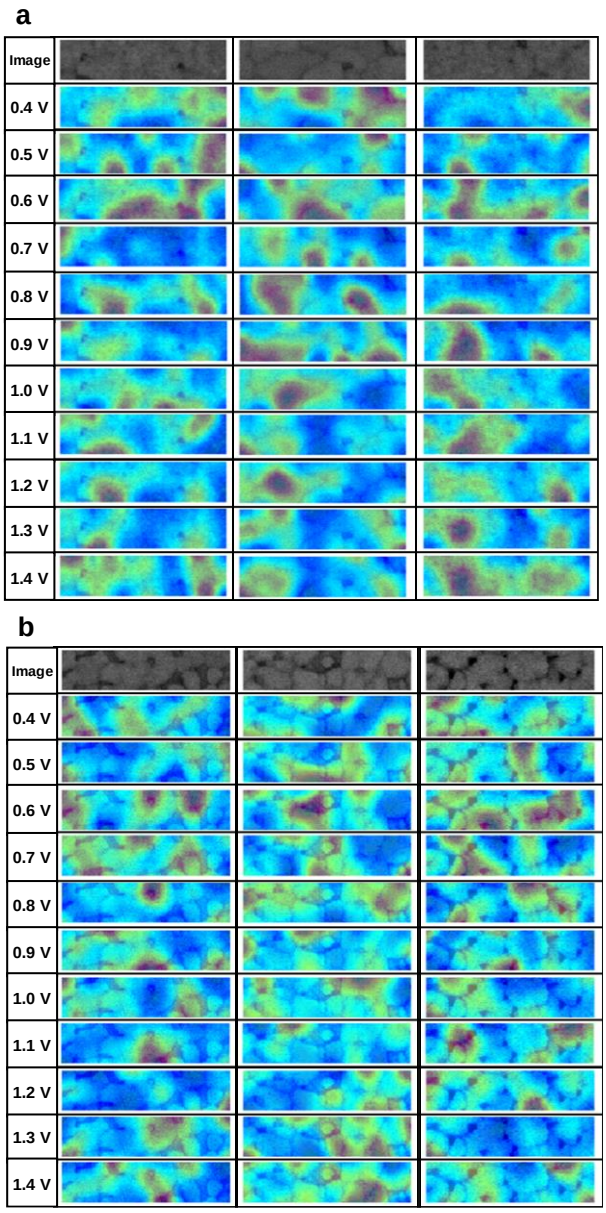

Fig. S12.

LIME activity images are shown for the SEM images (×10000) for the samples with the highest and lowest photocurrent. The highest and lowest 3 images were selected, respectively. The first row shows the original SEM images (BEI) for comparison with the LIME activity images. The left column shows the original SEM images. From the second row to the right, the activity images for the prediction of the photocurrent at different bias voltages (0.4 to 1.4 V).

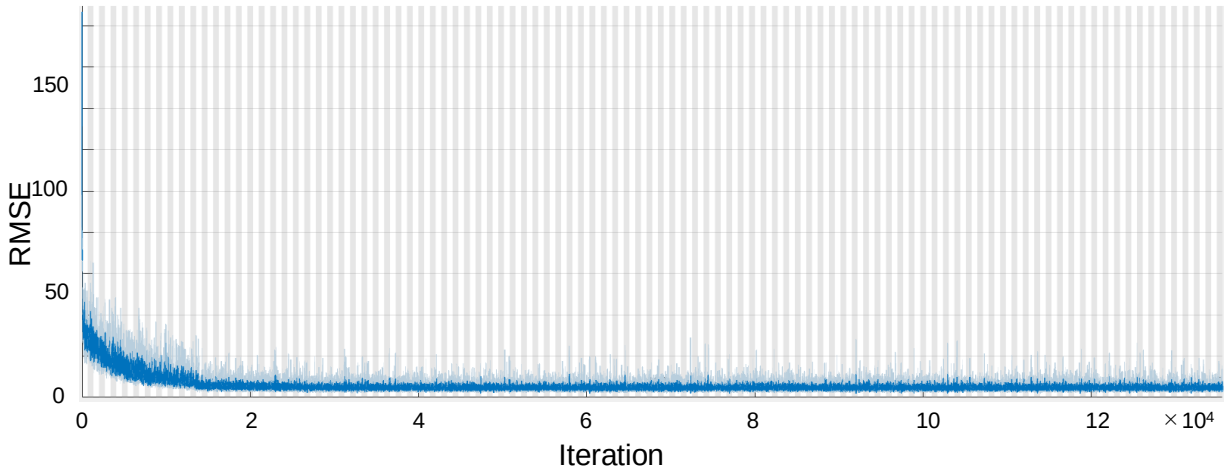

Fig. S13.

A typical training curve is shown, where the CNN model is adjusted to the J-V curve. The overlay of BEI and SEM images were used as input. The learning rate was 1×10^{-5}, and the epoch was 100. The root mean square error (RMSE) was reduced during the training.